# Photoassisted Scanning Tunneling Microscopy and Tunneling Spectroscopy of n-Type Tungsten Diselenide (n-WSe₂) Single Crystals

**Fu-Ren F. Fan and Allen J. Bard***

*Department of Chemistry and Biochemistry, The University of Texas at Austin, Austin, Texas 78712*

*Received: August 14, 1992; In Final Form: November 4, 1992*

The van der Waals surface (perpendicular to the *c* axis) of a nondegenerate n-type WSe₂ single crystal was imaged at negative substrate bias voltage ($V$) in the constant-current mode in air with a scanning tunneling microscope (STM) combined with optical excitation techniques. A current ($i$) image at a positive bias under steady-state illumination, obtained simultaneously with the topographic image, revealed that the photocurrent at the step edges was much smaller than that in the defect-free region. This reduction of the photocurrent at defect sites is attributed to a high surface recombination rate at defects. Tunneling spectroscopy (TS) performed in N₂, including $i$ vs $V$ and $di/dV$ vs $V$ curves with the tip held over the n-WSe₂ surface, was also carried out both in the dark and under laser irradiation. The results were interpreted in terms of the band locations and minority carrier injection through photoexcitation.

## Introduction

Transition-metal dichalcogenides have been used as semiconductor electrodes in photoelectrochemical (PEC) cells.[1] The behavior and efficiencies of these cells depend strongly on the nature of the electrode surface.[2-6] Scatter in the electrochemical (EC) parameters and the PEC behavior found in such cells by different laboratories can be attributed to significant sample-to-sample variations in the morphology of the WSe₂ crystals employed as electrodes. For example, the presence of exposed edges on the van der Waals surface leads to significant dark anodic currents at n-type electrodes and lower photocurrent efficiencies.[2c,5a] Thus, methods of examining the surface to characterize defects on semiconductors exposed to gaseous or liquid environments, and especially techniques capable of high spatial resolution, are very useful. For example, Parkinson and co-workers[7] have successfully used a scanning laser system in a PEC cell to identify semiconductor surface topological features and to correlate these features to the carrier collection efficiency. The scanning tunneling microscope (STM)[8] can also be used in measurements of irradiated semiconductor surfaces by combining STM with optical techniques.[9] This new method can provide spectroscopic information about the surface and near-surface region with high spatial resolution.

Since cleaved surfaces of WSe₂ are atomically flat and inert to oxidation, this semiconductor is especially suitable for tunneling microscopy experiments.[10-14] Akari et al.[10] recently reported preliminary results on the photoaction spectra of p-WSe₂ with an STM. Information about energy-dependent creation and recombination of charge carriers in the vicinity of the surface can be obtained by photoassisted tunneling spectroscopy (PATS) without the necessity of covering the surface with a conducting film.

In this paper, as an extension of our STM and tunneling spectroscopy (TS) studies on n-TiO₂ (001)[15a] and n-FeS₂ (001) surfaces,[15b] we report a series of experiments involving TS measurements of a tunnel junction consisting of a metal tip and an n-WSe₂ substrate in the dark and under laser irradiation. The differential conductance spectra obtained in the dark and under illumination are compared. The light-induced excess (photo) current was found to vary spatially, with large decreases occurring at step edges where there are higher rates of recombination of the charge carriers. The short-circuit photocurrent ($i_{sc}$) and open-circuit voltage ($V_{oc}$) (under laser irradiation) depended on the distance between the tip and the substrate.

## Experimental Section

The n-WSe₂ single crystals were grown by the vapor-transport method.[16] The resistivities of the crystals ranged from 0.1 to 0.2 Ω cm. To prepare fresh WSe₂ surfaces, the top layers of the bulk crystals were peeled off with adhesive tape in the air. The thin WSe₂ layers used in the back-illumination experiments were prepared by peeling them off of a bulk crystal with tape, which was then removed from the thin layer by dissolving the tape in methylene chloride. The optical transmission of these thin WSe₂ layers at 632.8 nm ranged from 1% to 10% (corresponding to thicknesses of ca. 0.1–0.2 μm).[17] Ohmic contacts were made by rubbing In–Ga alloy on the outside edges of the crystal. An electrical lead was then connected to the contact with conductive silver paint (Acme Chemicals & Insulation Co., Allied Products Corp., New Haven, CT). The electrode was covered, along with the contact and all sides of the crystal, except for an exposed area of ca. 0.01 cm², on the surface with insulating epoxy. The electrodes studied here showed mirrorlike surfaces with no obvious edges and pits on the surfaces when examined at a magnification of 200×.

The STM apparatus and the detailed procedures for current and differential conductance measurements have been described previously.[15] Briefly, current images (constant height) were obtained by stabilizing the feedback loop at a bias voltage of –1.0 V (in all cases reported, bias is that of the substrate vs tip) and with a reference current of 0.1 nA and then interrupting the feedback loop and measuring the tip current at the desired bias at each location. In TS measurements, after interruption of the feedback loop, the bias voltage ($V$) was swept linearly at ca. 2 V/s and the current ($i$) was recorded to obtain the $i$–$V$ curve. A 10–20-mV peak-to-peak sinusoidal signal ($\Delta V$) at 10 kHz was superimposed on the dc ramp, and the variation in the in-phase current ($\Delta i$) was determined with a lock-in amplifier to obtain the differential conductance, $di/dV$, as a function of $V$. All conductances reported here represent the differential conductance, unless otherwise indicated.

Electrochemically etched Ir–Pt tips (FHC Co., Brunswick, ME) were employed. All experiments, unless indicated otherwise, were performed under N₂, either in the dark or under irradiation with an 8 mW He–Ne laser (Spectra-Physics Inc., Mountain View, CA). The experiments in N₂ were performed by keeping the STM unit in a machined Plexiglas chamber, which was continuously purged with purified N₂.

## Current–Voltage Curves
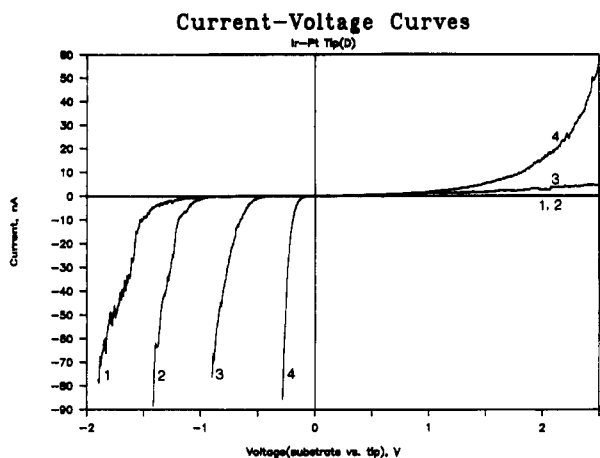


**Figure 1.** Current vs voltage curves in the dark for an Ir–Pt tip and an n-WSe$_2$ sample at various tip–sample separations. 1: reference tip–sample separation ($s_0$) defined by a current 0.5 nA at bias voltage –1.0 V. 2: $s_0$ –5 Å. 3: $s_0$ –10 Å. 4: $s_1$ for $i$ = 0.5 nA and $V$ = –0.1 V.

## Results

**Current–Voltage Relation in the Dark.** In Figure 1, the experimentally determined $i$–$V$ relationships in the dark at various tip–substrate separations, $s$, are shown. Since the absolute value of the tip–substrate gap cannot be determined, a relative separation, at a designated reference current and bias voltage, was arbitrarily taken as the reference gap [e.g., $s_0$ for $i$ = 0.5 nA at $V$ = –1.0 V (curve 1) and $s_1$ for $i$ = 0.5 nA at $V$ = –0.1 V (curve 4)], and other distances are given with respect to this gap. As shown in this figure, the magnitude of the current at a given bias strongly depends on $s$. At a given $s$, the current depends strongly on the bias voltage, and the $i$–$V$ curves display very asymmetric (Schottky diodelike) behavior. Note that for a given voltage magnitude, the current is much larger at negative bias than at positive bias. In the negatively biased voltage region, at large $s$ (curves 1 and 2), the $i$–$V$ curves were not smooth and showed several shoulders near –1.5 V. As $s$ decreased, the $i$–$V$ curves became fairly smooth and approached a nearly exponential dependence at large bias (curve 4). In the positive-bias region, essentially no current could be detected when $s$ was large (curves 1 and 2), while at smaller gaps significant current was observed when the bias was greater than 0.5 V (curves 3 and 4). The magnitude of the current in this region, as compared with the $i$–$V$ curves in the negative-bias region, was less dependent on $s$.

**Conductance–Voltage Relation in the Dark.** Figure 2 shows the differential conductance (d$i$/d$V$) spectra over the bias voltage range of –1.5 to +1.7 V for two different gap separations ($s_0$ and $s_1$). At the larger gap ($s_0$), the differential conductance was very low in the positive-bias region (curve 1). In the negative-bias region, the d$i$/d$V$ spectrum showed a peak near –1.4 V where a shoulder was observed in the $i$–$V$ curves. At the smaller gap, $s_1$, the differential conductance in the positive-bias region was greatly enhanced. As shown in curve 2, two well-defined peaks can be identified: a prominent symmetric peak with a half-height width of ca. 0.2 eV at ca. 0.8 V and a broader peak located at ca. 1.5 V. Following this broad peak, the differential conductance increases again with increasing bias. In the negative-bias region, high differential conductance was observed even at the larger distance.

**Current–Voltage Relation under Irradiation.** Figure 3 shows two $i$–$V$ curves at a gap defined by –1.0 V and 0.28 nA, one in the dark and the other under front surface illumination at a glancing angle (nearly parallel to the surface of the n-WSe$_2$ electrode). In the dark, no current was observed at a bias voltage positive of ca. –0.5 V. When illuminated, however, a photocurrent was observed in the positive-bias region. Thus, a short-circuit photocurrent, $i_{sc}$, of ca. 2 nA and an open-circuit photovoltage, $V_{oc}$, of ca. 0.5 V were obtained under illumination. This large

## Conductance Spectra of n-WSe2 in the dark
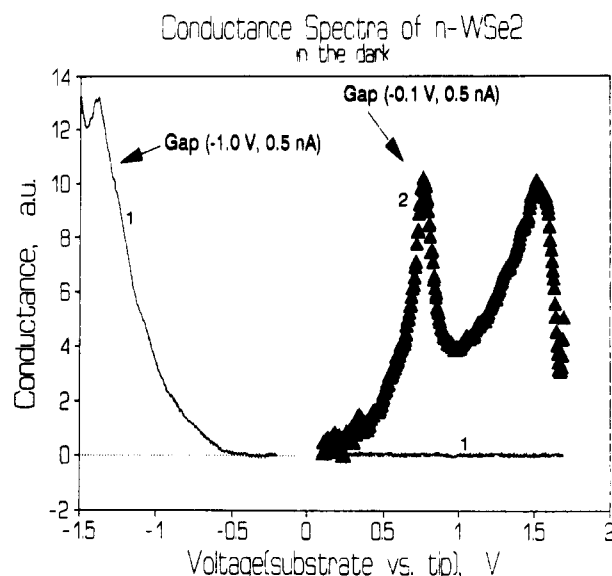


**Figure 2.** Differential conductance (d$i$/d$V$) as a function of voltage for an Ir–Pt tip and an n-WSe$_2$ sample at two gap separations ($s_0$ and $s_1$). Modulation frequency of 10 kHz and modulation amplitude of 20 mV peak-to-peak were used in the phase-sensitive technique at distance 1, $s_0$ (–1.0 V, 0.5 nA), and 2, $s_1$ (–0.1 V, 0.5 nA).

## Current–Voltage Curves of n-WSe2 in the dark & under front illumination
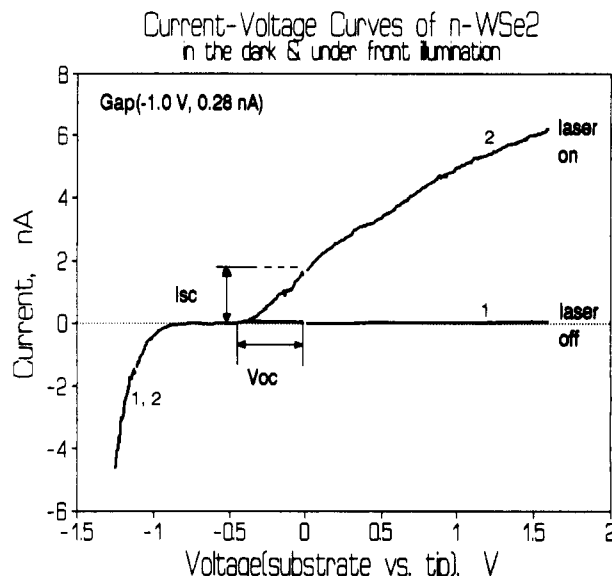


**Figure 3.** Current vs voltage curves for an Ir–Pt tip and a different n-WSe$_2$ sample at gap separation (–1.0 V, 0.28 nA). 1: In the dark. 2: Under front surface illumination at a glancing angle. $i_{sc}$, short-circuit current under illumination; $V_{oc}$, open-circuit voltage under illumination.

open-circuit voltage could not be attributed to the thermoelectric voltages generated by the differential heating of the tunnel junction by the absorbed radiation. Such thermoelectric voltages are usually small (a few millivolts).[9b] Moreover, we do not expect the thermoelectric current to vary as much with the bias voltage as is shown here. To eliminate possible effects of diffraction and shadowing by the tip, most of the later photoexcitation experiments were performed with back-illumination (through the WSe$_2$ layer). In Figure 4, the experimentally observed $i$–$V$ relationships in the dark and under back-illumination at two tip–substrate gaps, e.g., $s_2$ (–0.1 V, 0.1 nA) and $s_3$ (–1.0 V, 0.1 nA) are shown. At the larger gap (i.e., $s_3$), no current flow was observed in the dark at bias voltages positive of –0.7 V (curve 4). Under illumination, little change in the current was observed until the bias voltage was positive of 0 V. At the smaller gap ($s_2$), the photocurrent rose sharply at a bias of –0.1 V and tended to level off at biases above 0 V. At a bias positive of 0.5 V, the photoinduced current was superimposed on a high increasing background dark current,
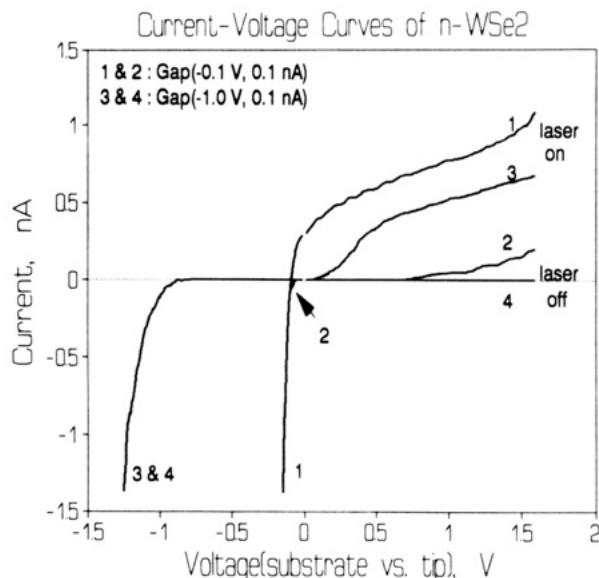
**Figure 4.** Current vs voltage curves for an Ir–Pt tip and a different n-WSe$_2$ sample. 1: Under back-illumination at gap $s_2$ (–0.1 V, 0.1 nA). 2: In the dark at gap $s_2$. 3: Under back-illumination at gap $s_3$ (–1.0 V, 0.1 nA). 4: In the dark at gap $s_3$.

**TABLE I: Open-Circuit Voltage ($V_{oc}$) and Short-Circuit Current ($i_{sc}$) as Functions of Gap under Back-Illumination**

| gap, Å | $V_{oc}$, V | $i_{sc}$, nA |
|---|---|---|
| $s_2$ (–0.1 V, 0.1 nA) | 0.10 | 0.32 |
| $s_2$ +5 | 0.25 | 0.25 |
| $s_2$ +15 | 0.12 | 0.05 |
| $s_3$ (–1.0 V, 0.1 nA) | 0.0 | 0.00 |

which was found for different crystals (e.g., see curves 3 and 4 of Figure 1). Also shown in Figure 4 is the strong dependence of $V_{oc}$ and $i_{sc}$ on $s$. Table I summarizes $V_{oc}$ and $i_{sc}$ as functions of gap. Notice that $i_{sc}$ decreases steadily with increasing gap separation, while $V_{oc}$ first increases to reach a maximum and then decreases with increasing $s$.

**Conductance–Voltage Relation under Irradiation.** Figure 5 shows the characteristic $di/dV$ spectra of an n-WSe$_2$ electrode at larger $s$ in the dark (curve 1) as well as with back-illumination (curve 2). The differential conductance in the voltage range negative of ca. –0.3 V changed only slightly with irradiation. However, the radiation enhanced dramatically the differential conductance for a bias more positive than –0.3 V, where no conductance was observed in the dark with this sample at the same gap. A photoinduced conductance peak is seen at ca. 0.3 V, where the rate of the photocurrent change with respect to the bias reached a maximum (see curve 3 of Figure 4).

**STM Images.** In Figure 6A, we show a 128-nm × 128-nm constant-current topographic image of an n-WSe$_2$ surface in air acquired at a bias voltage of –1.0 V and a reference current of 0.1 nA. During imaging, the sample was under steady-state back-illumination with a He–Ne laser. The overall morphology of the surface is fairly smooth, but several steps are seen near the middle portion of the image. A similar topographic image (not shown) was obtained in the dark at this negative bias. In Figure 6B, we show the current image acquired simultaneously with the topograph shown in Figure 6A but with a bias voltage of 0.5 V. This was obtained during current imaging, by periodically interrupting the feedback loop, switching the bias voltage from –1.0 to +0.5 V, and measuring the current. Because the current at step edges is smaller than that on the plane, a conventional presentation of current as a function of position would hide these lower current values. To show these in the image, the current values were inverted (multiplied by –1) and then rotated 180° to present lower currents in the downward direction. At a bias voltage of 0.5 V, no dark current, but substantial photocurrent,
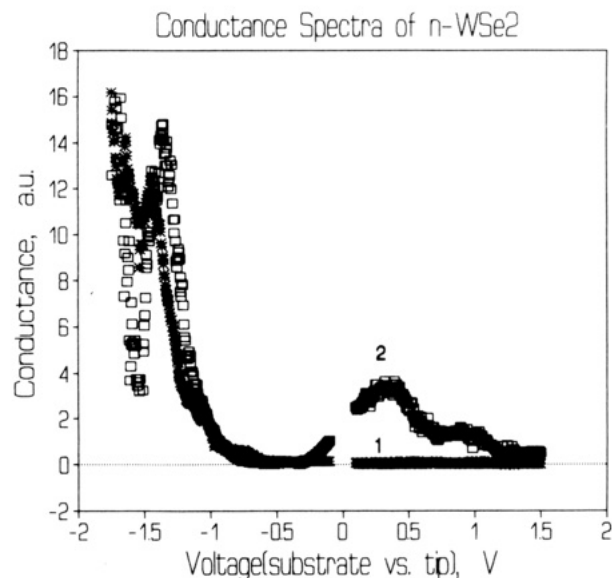


**Figure 5.** Differential conductance as a function of voltage for an Ir–Pt tip and the n-WSe$_2$ sample in Figure 4 at gap separation $s_3$. 1: In the dark. 2: Under back-illumination. Modulation frequency, 10 kHz, and amplitude, 20 mV, as in Figure 2.
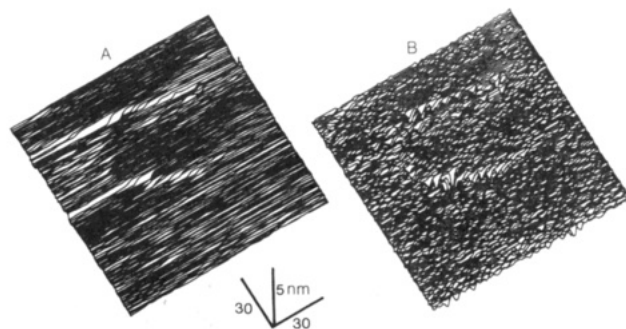


**Figure 6.** (A) 128-nm × 128-nm constant-current topographic image of the n-WSe$_2$ sample used in Figures 4 and 5. The image was acquired in air at a bias voltage of –1.0 V and a reference current of 0.1 nA. During imaging, the sample was under steady-state back-illumination with an 8-mW He-Ne laser. (B) Current image acquired at a sample bias of 0.5 V under steady-state back-illumination. The feedback loop was interrupted during current imaging. The current range is from 0 to 0.45 nA. The original current image has been inverted and rotated 180° to obtain the present reverse hidden line image. This format shows the data that are not seen in the normal format because they are underneath and behind the data in the front.

was observed (see curves 4 and 3 of Figure 4). The photocurrent was higher on the smooth surface of the crystal and much lower on the step edges and exposed defects.

### Discussion

**Current and Conductance Measurements in the Dark.** The observed results can be interpreted by the model for charge transfer at a metal/insulator/semiconductor (MIS) junction discussed previously,[15b] although a more realistic model that accounts for the effect of curvature of the tip on the distribution of electric field would be required for quantitative analysis. In this model, we also neglect a possible nonequilibrium condition which might be created in the reverse-bias region (i.e., a positive bias with an n-type semiconductor) where depletion of the minority carriers (holes) might take place during tunneling of electrons from the tip. However, in a later discussion, we will reconsider this situation. On the basis of this MIS model, one can show the voltage change across the tip/semiconductor gap, $\Delta V_i$, as a function of applied voltage in the absence of surface states (Figure 7).[15b,18] The distribution of the applied potential between the gap ($\Delta V_i$) and across the semiconductor depends upon the
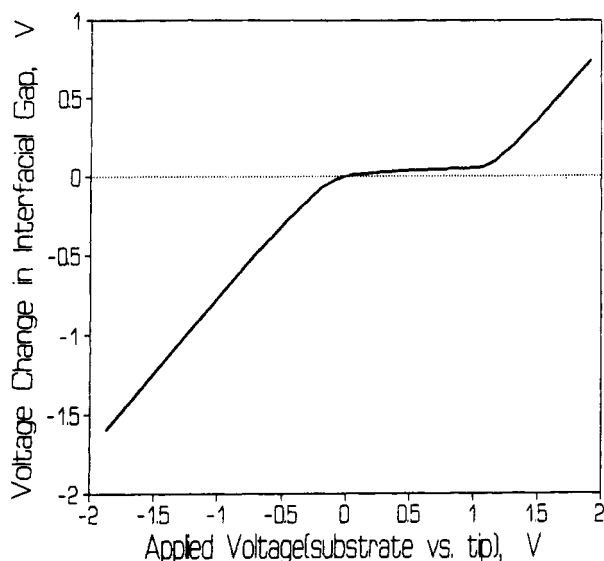
**Figure 7.** Change in the voltage across the tip–substrate gap as a function of applied bias voltage. The following parameters have been used to calculate the curve: bulk electron density, $n_b = 2.0 \times 10^{23}$ m$^{-3}$; bulk hole density, $p_b = 2.26 \times 10^{7}$ m$^{-3}$; permittivity of WSe$_2$, $\epsilon_s = 10\epsilon_0$; permittivity of air gap, $\epsilon_i = \epsilon_0$ ($\epsilon_0$: the permittivity of free space); $s = 2.0$ nm; energy gap of WSe$_2$, $E_g = 1.16$ eV. No initial band bending was assumed.

**SCHEME I**
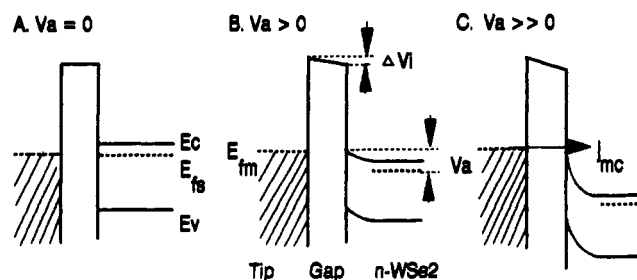


**SCHEME II**
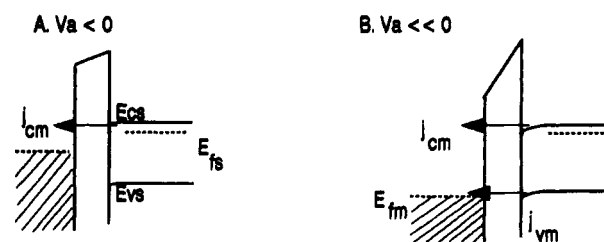


magnitude of the bias. As the potential of n-WSe$_2$ is made more positive (with respect to the flat band condition), the applied bias largely is taken up by the potential drop across the space charge region, as shown in Figure 7 (see Scheme I). As mentioned previously, the presence of surface states can often significantly affect $\Delta V_i$, depending on the nature, energy location, and density of these states. Several interesting conclusions can be drawn from the MIS model based on the information shown in Figure 7. First, in the negative-bias region, the applied voltage drops nearly across the insulating gap and is essentially independent of the donor concentration as long as it is greater than $10^{21}$ m$^{-3}$. In this regime, the conductance at low bias (see Figure 2) is associated with the electron flow from the conduction band of n-WSe$_2$ to the tip, $J_{cm}$, (Scheme IIA). A further increase in the magnitude of the negative bias causes electrons to accumulate at the surface of n-WSe$_2$. This causes the Fermi level of the tip, $E_{fm}$, to move downward relative to the semiconductor until it reaches the valence band edge, $E_{vs}$, of n-WSe$_2$ at the surface. At this point, the electron flow from the valence band of n-WSe$_2$ to the tip, $J_{vm}$, increases rapidly with bias (Scheme IIB). For the n-WSe$_2$ crystals

studied here, the applied voltage necessary to reach this condition was about $-1.2$ V. Second, in the positive-bias region, the large concentration of positive charges required for a strong electric field across the (tip/substrate) gap is provided by ionized donor and gap states, and this causes $E_{fm}$ to move upward above the conduction band edge of n-WSe$_2$, $E_c$, at which point electron flow from the tip to the conduction band of n-WSe$_2$, $J_{mc}$, becomes large (Scheme IC). This results in the increasing current observed at large positive-bias voltage shown in Figure 1. This current cannot be mainly attributed to the electron flow from the tip to the valence band of n-WSe$_2$, $J_{vm}$, since it depends on the surface concentration of holes which in turn depends on the relatively voltage-independent bulk and space charge region thermal generation rates.

It is interesting to notice that the applied voltage needed to move $E_{fm}$ to and above the $E_c$ of n-WSe$_2$ is very sensitive to the doping level.[18] For the n-WSe$_2$ crystals studied here ($n_b \approx 4 \times 10^{23}$ m$^{-3}$), it is larger than 1.0 V for a gap separation of 2.0 nm with respect to the contact point. Thus, the width of the theoretical low-conductance region is considerably greater than the band gap of WSe$_2$ (which is ca. 1.16 eV[5b]) because of band bending.

Different processes could give rise to the conductance peaks shown in Figure 2. First, they might be associated with electron transfer between the tip and the energy bands of the semiconductor. In this case, the slowly-increasing conductance observed in the low-negative-bias region, as observed for most n-type semiconductors, is attributed to $J_{cm}$. The conductance peaks in the highly-negative-bias region (as shown in Figures 2 and 5) may be associated with electron transfer between the tip and the fairly localized uppermost valence level consisting of W (5d) states, as suggested by the theoretical calculations of the band structure.[19] The well-defined conductance peaks in the highly-positive-bias region is attributed to electron flow from the tip to the conduction band manifold of n-WSe$_2$, $J_{mc}$. The experimentally observed d$i$/d$V$ spectrum agrees qualitatively with the computed band structure; however, a quantitative analysis is, as suggested above, complicated by the band bending.

The second mechanism responsible for the conductance peaks involves states within the energy gap. The conductance peak which might be associated with this mechanism is the one located at a bias of ca. 0.8 V as shown in Figure 2. Since at the bias voltage of 0.8 V $E_{fm}$ is near the conduction band edge of n-WSe$_2$, any gap states are opposite a very high concentration of electrons in the tip. If the gap states exchange electrons with the tip more rapidly than they do with the semiconductor bands, they would remain filled with electrons and the change in charge called for by the applied voltage would have to occur in the space charge layer. One would expect that the junction would behave like a Schottky barrier whose current and conduction would be nearly independent of the tip–substrate gap, $s$, over the bias region near 0.8 V. This is apparently not what is experimentally observed. Thus, to obtain the $s$-dependent charge-exchange conductance, one must assume that these gap states have much better communication with the semiconductor bands than with the tip. This assumption is justified by the experimental observation that no significant well-defined conductance peak in the negative-bias region was observed near $-0.8$ V, where $E_{fm}$ is aligned with the gap states (see Figure 2). The conductance at a fixed frequency could peak at the bias voltage when the semiconductor Fermi level is aligned with the gap states. From the relation of the surface potential of the semiconductor as a function of applied voltage, one can estimate the energetic location of these gap states at ca. 0.2 eV above the top of the valence band of n-WSe$_2$. The slow or negligible exchange rate between the tip and the gap states further suggests that they are probably not located at the tip/gap interface. The mechanism for the formation of these states is still rather unclear but might be associated with the high electric field strength and tip force at the interface.
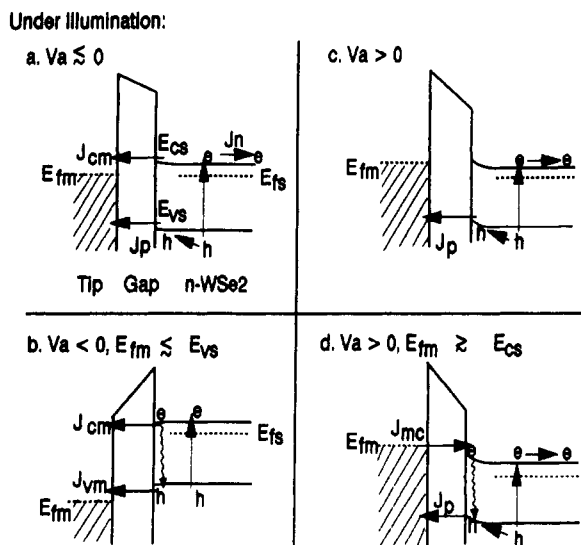
**Figure 8.** Energy band diagrams for n-type MIS structures showing potential distribution under different bias conditions and under irradiation. The wavy arrows indicate electron (e)–hole (h) recombination. $E_{fm}$ is the Fermi level in the bulk of the tip; $E_{fs}$ is the Fermi level of the semiconductor in the bulk; $E_{cs}$ and $E_{vs}$ are the conduction band and valence band edges of the semiconductor at the surface; $V_a$ is the applied voltage; and $J_p$ is the photogenerated current.

Another mechanism responsible for the conductance peaks might involve inversion and tunneling of electrons from the tip to valence band. However, inversion apparently does not occur under the present experimental conditions. The large current and conductance observed at high-negative-bias voltage, where $J_{vm}$ was significant (Scheme IIB), and the small nearly-saturated current observed in the positive-bias region, where $J_{mc}$ was the dominant conduction process (Scheme IC), indicate that the hole-transfer rate between the tip and the valence band of n-WSe$_2$ is much faster than the rate of thermal generation of holes in the semiconductor. Thus, holes will be depleted at the surface of n-WSe$_2$.

**Current and Conductance Measurements under Illumination.** Concerning the photoeffect on the conductance spectrum, we first focus on the differential conductance observed in the low-bias region. As shown in Figure 5, a conductance peak was observed at ca. 0.3 V when *s* was large. This conductance peak and its corresponding photocurrent (see Figure 4) are clearly associated with photogenerated carriers, since no current and conductance were observed in the dark in this voltage region. Thus, we attribute these features to the photoenhanced electron transfer between the tip and the valence band of n-WSe$_2$ (see Figure 8a and 8c). These results indicate that the negligibly small magnitude of $J_{mv}$ observed in the dark (as suggested by curves 1 and 2 of Figure 1) is mainly due to the small concentration of holes at the surface of n-WSe$_2$. This further implies that the thermal (dark) generation rate of holes in the bulk and space charge region is rather low, as discussed above. Note that as the bias continues to increase, the photoenhanced differential conductance decreases mainly because the photocurrent reaches a steady-state value which is controlled by the light intensity and the diffusion of the photogenerated holes to the interface. Thus, the rate of change in the photocurrent with respect to the bias voltage first reaches a maximum and then decreases with increasing bias. Moreover, the increase in the positive bias also increases $J_{mc}$, which in turn decreases the concentration of photogenerated holes through recombination inside the semiconductor, and thus decreases the photoinduced conductance (see Figure 8d).

Notice also that the d*i*/d*V* spectrum under illumination also shows a shoulder at ca. 0.9 V (see Figure 5). This small shoulder might be associated with the states responsible for the conductance peak at ca. 0.8 V observed in the dark at small *s*. At large *s*, no

conductance was observed in the dark due to low concentration of holes at the surface of n-WSe$_2$. However, irradiation enhances the hole concentration inside the semiconductor and thus increases the hole population of the states.

Under open-circuit conditions, for an MIS tunnel junction at steady state, the current of minority carriers (holes for an n-type semiconductor) produced by illumination is compensated by an equal flow of majority carriers. For an MIS tunnel device,[20]

$$V_{oc} = n(k_B T/q)[\ln (J_{sc}/J_{no} + \chi^{1/2}s)] \qquad (1)$$

where *n* is the diode nonideality factor under illumination; $k_B$, the Boltzmann constant; *T*, the absolute temperature; *q*, the charge of the electron; $J_{no}$, the reverse saturation current; and $\chi^{1/2}s$, the tunnel exponent.

As predicted by eq 1, the presence of an interfacial gap, *s*, can affect $V_{oc}$ through the tunnel exponent $\chi^{1/2}s$ and the nonideality factor *n*, since in the low-bias region, where the photoeffect is of most interest, the bias voltage is mainly dropped across the space charge layer. If the doping density is not very high, *n* can be treated as a constant. Thus, $V_{oc}$ is mainly affected by *s* through the factor $\chi^{1/2}s$ for majority carriers. For an ideal MIS device, when *s* is small, $J_{sc}$ decreases only slightly with increasing *s*. This makes $V_{oc}$ first increase with increasing *s*. As *s* continues to increase, a point is reached beyond which the diffusion current of the photogenerated minority carriers begins to decrease dramatically due to the series resistance of the interfacial gap. At this point, $V_{oc}$ begins to drop with *s*. Our experimental results, as shown in Table I, agree qualitatively with this prediction.

**Images under Illumination.** Exposed edges of layer-type compounds have been shown to act as recombination centers for charge carriers and cause lower photocurrent efficiencies.[2c,5a,7] As clearly shown in Figure 6A, a number of atomic steps exist near the middle portion of the image. The corresponding photocurrent image (Figure 6B) shows that the photocurrent is much lower at the step edges and exposed defects than on the smooth surface. This is consistent with the previous PEC observations and the results of scanning laser spot experiments.

**Conclusions**

We have demonstrated that for a tip/gap/n-WSe$_2$ junction consisting of a nondegenerate n-WSe$_2$ crystal with a small gap, a nonequilibrium situation occurs which results in an asymmetric *i–V* characteristic. The saturation in current in the reverse-bias region (i.e., with a positive sample bias for the present n-type material) can be eliminated by minority carrier (hole) injection through photoexcitation. The open-circuit voltage under illumination as a function of gap separation qualitatively follows that predicted for an MIS tunnel junction. Moreover, the information obtained by scanning tunneling spectroscopy provides new insight into the role of surface defects, e.g., exposed step edges, in carrier transport and surface recombination processes. The mechanism for the formation of these defect states is still rather unclear, however.

**References and Notes**

(1) Tributsch, H. *Struct. Bonding* **1982**, *49*, 127.
(2) (a) Fan, F.-R. F.; White, H. S.; Wheeler, B.; Bard, A. J. *J. Am. Chem. Soc.* **1980**, *102*, 5142. (b) Fan, F.-R. F.; Bard, A. J. *J. Electrochem. Soc.* **1981**, *128*, 945. (c) White, H. S.; Fan, F.-R. F.; Bard, A. J. *Ibid.* **1981**, *128*, 1045.
(3) Parkinson, B. A.; Furtak, T. E.; Canfield, D.; Kam, K.; Kline, G. In *Faraday Discussions of the Chemical Society*; No. 70; The Royal Society of Chemistry: London, 1980; p 233.
(4) Lewerenz, H. J.; Heller, A.; DiSalvo, F. J. *J. Am. Chem. Soc.* **1980**, *102*, 1877.
(5) (a) Ahmed, S. M.; Gerischer, H. *Electrochim. Acta* **1979**, *24*, 705. (b) Kautek, W.; Gerischer, H. *J. Electrochem. Soc.* **1980**, *127*, 2471.

(6) (a) Schneemeyer, L. F.; Wrighton, M. S. *J. Am. Chem. Soc.* **1979**, *101*, 6496. (b) Schneemeyer, L. F.; Wrighton, M. S.; Stacy, A.; Sienko, M. J. *Appl. Phys. Lett.* **1980**, *36*, 701.

(7) Furtak, T.; Canfield, D.; Parkinson, B. A. *J. Appl. Phys.* **1980**, *51*, 6018.

(8) Binnig, G.; Rohrer, H. *Helv. Phys. Acta* **1982**, *55*, 726.

(9) See, e.g.: (a) Van de Walle, G. F. A.; Van Kempen, H.; Wyder, P.; Davidson, P. *Surf. Sci.* **1987**, *181*, 356. (b) Kuk, Y.; Becker, R. S.; Silverman, P. J.; Kochanski, G. P. *Phys. Rev. Lett.* **1990**, *65*, 456. (c) Cahill, D. G.; Hamers, R. J. *J. Vac. Sci. Technol.* **1991**, *B9*, 564.

(10) (a) Akari, S.; Lux-Steiner, M. Ch.; Vögt, M.; Stachel, M.; Dransfeld, K. *J. Vac. Sci. Technol.* **1991**, *B9*, 561. (b) Möller, R.; Akari, S.; Baur, C.; Koslowski, B.; Dransfeld, K. In *Scanned Probe Microscopy*; Wickramasinghe, H. K., Ed.; AIP Conference Proceedings No 241; American Institute of Physics: New York, 1992; p 314.

(11) Fuchs, H.; Laschinski, R.; Schimmel, T. H. *Europhys. Lett.* **1990**, *13*, 307.

(12) Akari, S.; Möller, R.; Dransfeld, K. *Appl. Phys. Lett.* **1991**, *59*, 243.

(13) Parkinson, B. *J. Am. Chem. Soc.* **1990**, *112*, 7498.

(14) Bolotov, L. N.; Derkach, B. E.; Ivantsov, L. F.; Makarenko, I. V.; Plekhanov, P. B.; Safarov, V. I. *Sov. Phys. Solid State* **1990**, *32*, 889.

(15) (a) Fan, F.-R. F.; Bard, A. J. *J. Phys. Chem.* **1990**, *94*, 3761. (b) *Ibid.* **1991**, *95*, 1969.

(16) Schäfer, H. *Chemical Transport Reactions*; Academic Press: New York, 1964.

(17) Frindt, R. F. *J. Phys. Chem. Solids* **1963**, *24*, 1107.

(18) Sze, S. M. *Physics of Semiconductor Devices*; Wiley: New York, 1981; Chapter 7.

(19) (a) Liang, W. Y. In *Physics and Chemistry of Electrons and Ions in Condensed Matter*; Acrivos, J. V., Mott, N. F., Yoffe, A. D., Eds.; NATO ASI 130; Dordrecht: Holland, 1984; p 459. (b) Coehoorn, R.; Haas, C.; Dijkstra, J.; Flipse, C. J. F.; de Groot, R. A.; Wold, A. *Phys. Rev.* **1987**, *B35*, 6195.

(20) Card, H. C. *Solid State Electron.* **1977**, *20*, 971.